

Status-reminder report on C-130 air-motion measurements
Test of DYCOMS-II new datasets

January 4, 2007

We remind and report here some problems that were observed in the in situ measurements of air velocity fluctuations on the NCAR C-130 aircraft during DYCOMS-II (also found during other experiments) and the impact of the recent two last re-processings of the dataset.

The following departures from their expected behaviour were noted on the spectra and the momentum fluxes in the original dataset:

1. The ratios between the transverse spectra and the longitudinal spectrum do not take the expected value of $4/3$ in the inertial subrange;
2. The vertical velocity spectrum follows a -2 slope rather than the predicted $-5/3$ slope in the inertial subrange;
3. The momentum fluxes seem to be biased by a spurious covariance between air vertical velocity and true airspeed, which is manifested in the component of momentum flux along the longitudinal axis of the airplane.

We find that the re-processing (mainly the new static pressure calibration) reduces the momentum flux bias to 21% of its previous value in the first new dataset and 17% in the second new dataset. However, the two other spectral inconsistencies (1. and 2.) remain in the new datasets. We observe very little difference between the two new datasets (first in summer 2005, second in fall 2006).

Notation:

u_a : True airspeed (*TASHC*),

u_p : Ground speed (function of *VEWC* and *VNSC*),

u : East component of the wind (*UIC*),

v : North component of the wind (*VIC*),

w : Vertical gust component (*WIC*),

u_x : Longitudinal component (*UXC*),

v_y : Lateral component (*VYC*),

u' : fluctuations of u ,

$\langle u'w' \rangle$: Covariance between u and w , calculated on 2.5 minutes segments.

The true heading angle chosen to represent each flux measurement is the true heading angle corresponding to the middle of the time segment.

The spectra calculation was also based on 2.5 minutes segments.

We discuss here the momentum fluxes and spectra calculated for the circles flown during DYCOMS-II for three kinds of datasets. The first is the dataset that was available to the DYCOMS-II community. The second is a re-processed dataset in summer 2005, with mainly a change of the static pressure calibration (static and dynamic pressure in the new run are dependent upon angle of attack instead of the raw QC) and true airspeed adjusted to account of small leak in the pitot/static system. The third is a re-processed dataset in fall 2006, with the same change of static pressure calibration, same adjustment of true airspeed to account of the leak in the pitot/static system and an additional corrective link between IRS and GPS ground speeds tightened up to 120 seconds - down from 600 seconds.

(That might be the only difference between the first and the second new datasets. To be confirmed by Allen.)

All boundary-layer circle legs of all flights are considered (RF0- 1, 2, 3, 4, 5, 7, 8).

Momentum fluxes

In the first set of figures, East and North components of the momentum fluxes, as well as the longitudinal and transverse components are displayed as a function of the true heading angle.

Calculating the momentum fluxes during DYCOMS-II along each circle of all the 7 flights, we found an unexpected dependence on the true heading angle for $\langle u'w' \rangle$ and $\langle v'w' \rangle$ in the original dataset (see Fig. 1). A real sinusoidal dependence on angle

around the circle of a given flight could be possible only if there were a real horizontal gradient of the flux. But the circle flown in the opposite direction should then show the exact opposite sinusoid. From one level to the other and from one flight to the other, the horizontal gradient would also likely have a different direction and would lead to different phase shifts in the sinusoid on different days. Therefore we would not expect see such a sinusoid when all the legs are combined.

This heading-dependence is due to a spurious covariance between the true air speed and the vertical velocity (Fig. 7, top panel). Since $u_x \approx u_a - u_p$, and since we do not observe the same covariance between the ground speed and the vertical velocity (Fig. 7, bottom panel), the covariance between u_a and w is manifested by a bias in $\langle u'_x w' \rangle$ (see also Fig. 10).

The equations

$$\langle u' w' \rangle = \langle u'_x w' \rangle \sin \psi - \langle v'_y w' \rangle \cos \psi \quad (1)$$

$$\langle v' w' \rangle = \langle u'_x w' \rangle \cos \psi + \langle v'_y w' \rangle \sin \psi \quad (2)$$

show that any bias in $\langle u'_x w' \rangle$ leads to a spurious sinusoidal signal in $\langle u' w' \rangle$ and $\langle v' w' \rangle$ as function of true heading angle.

A new static pressure calibration has been used in the new datasets. In the original dataset, the calibration is calculated as a linear function of the dynamic pressure. The new calibration of is calculated as a linear function of the ratio of the attack angle differential pressure to the dynamic pressure.

The covariance between u_a and w is reduced in the re-processed datasets (Fig. 8 and 9); therefore so is the bias of the longitudinal momentum flux $\langle u'_x w' \rangle$ (Fig. 5, 6, 11 and

12). Consequently, the spurious sinusoidal curve on the East and North component of the momentum fluxes is attenuated in the new datasets (Fig. 2 and 3) (to 25% of its previous value).

In the original dataset, we found a significant coherence between true air speed and vertical velocity around 0.3 Hz. Fig. 19 shows that this coherence is now much reduced in this range, but slightly increased at around 3 Hz.

Spectra

Fig. 16 shows that the new calibration attenuates the spectral energy of the longitudinal component in the same range of 0.3 Hz mentioned above, while the spectra of the lateral and vertical components are slightly changed by the new calibration, with more energy around 0.2 Hz. The observation of a steeper (than $-5/3$) slope for the vertical component and of a ratio close to 1 between transverse and longitudinal spectra rather than the theoretical $4/3$ (not shown), remain in the new dataset (Fig. 13, 14 and 15).

There are very small change from the first new dataset to the second new dataset, at very high frequency (Fig. 16, 17 and 18).

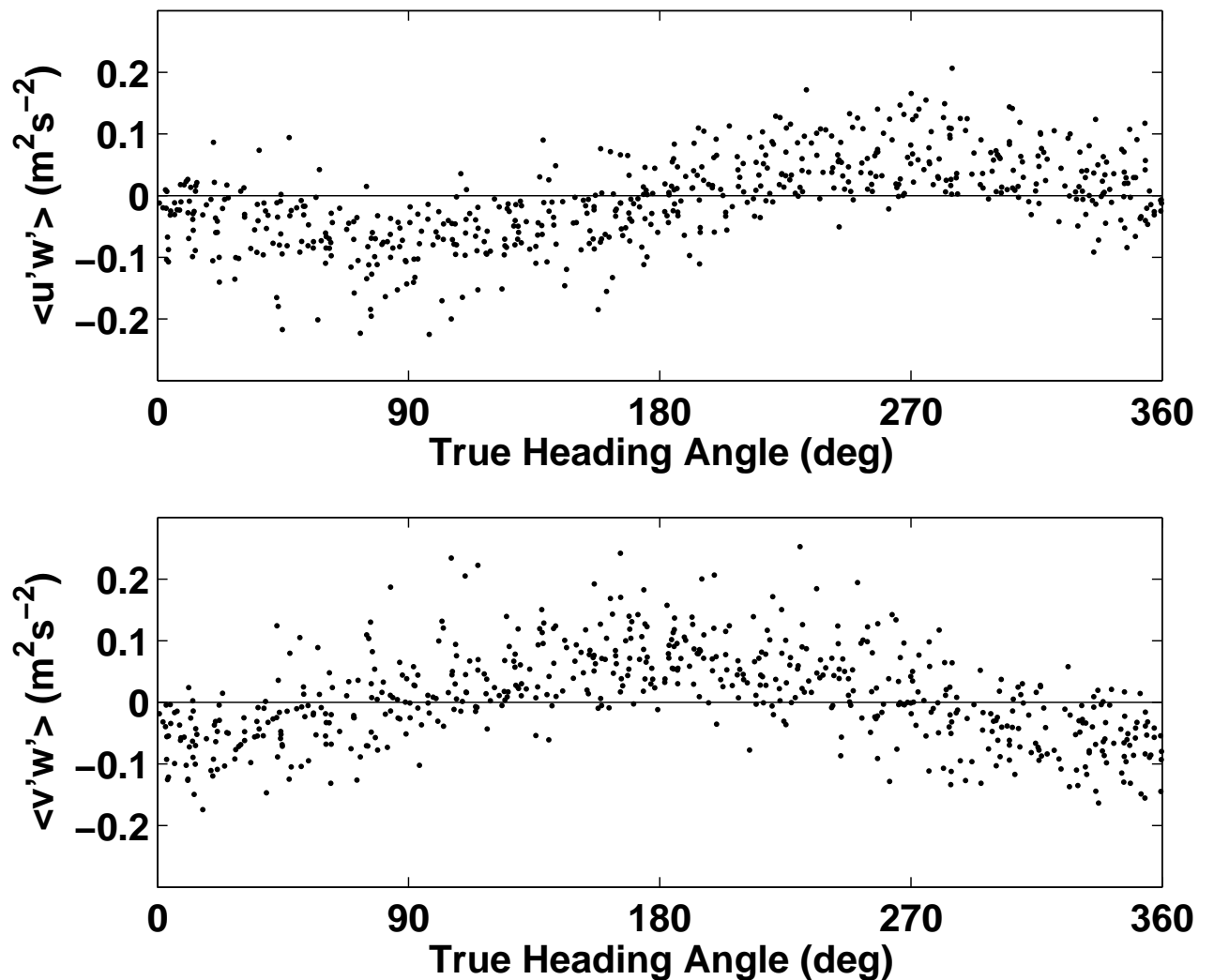


Figure 1: East (top) and North (bottom) components of the vertical momentum flux, as a function of the true heading angle, for all legs and all flights. Original dataset.

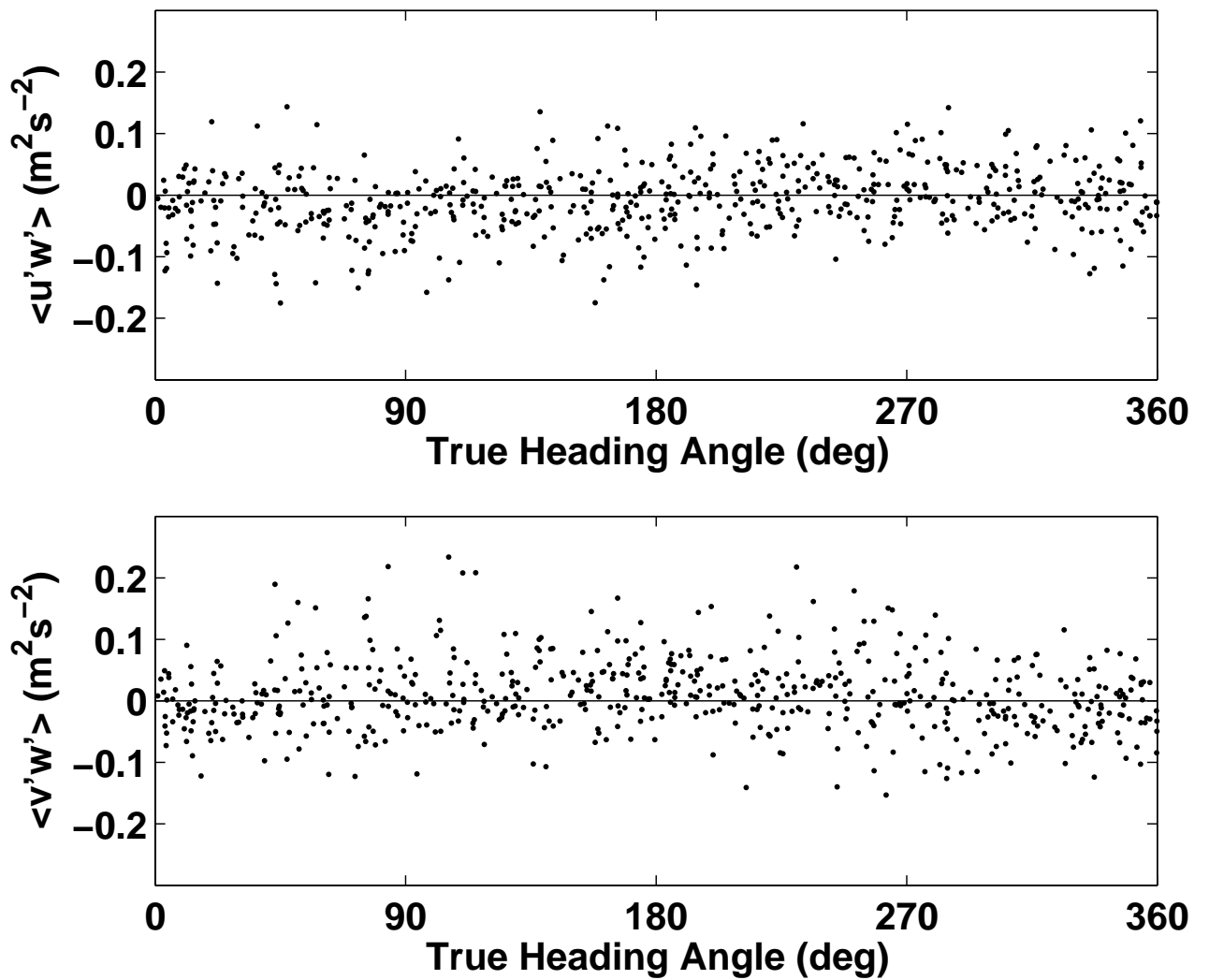


Figure 2: East (top) and North (bottom) component of the vertical momentum flux, as a function of the true heading angle for all legs and all flights. First new dataset (summer 2005).

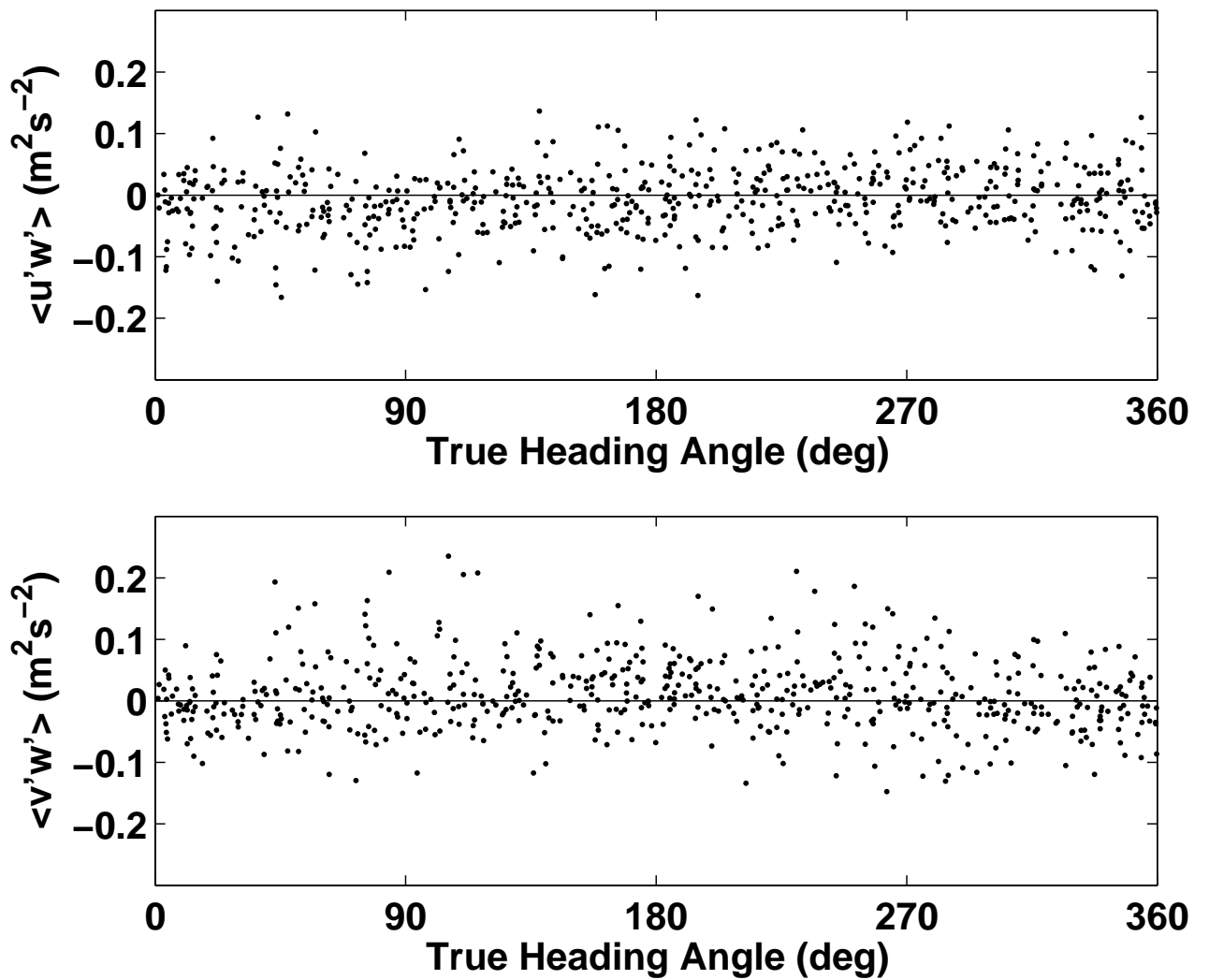


Figure 3: East (top) and North (bottom) component of the vertical momentum flux, as a function of the true heading angle for all legs and all flights. Second new dataset (fall 2006).

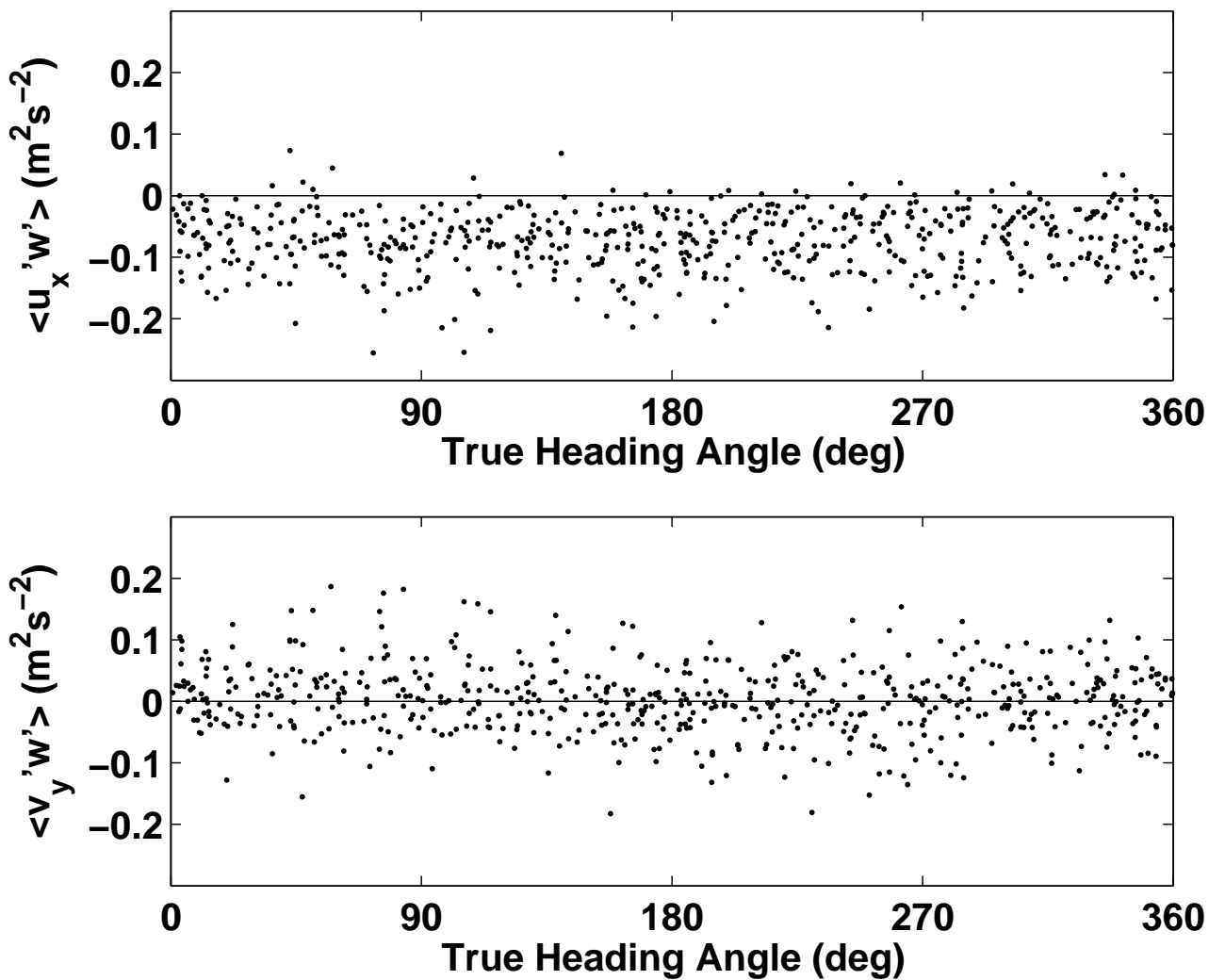


Figure 4: Longitudinal (top) and transverse (bottom) components of the vertical momentum flux, as a function of the true heading angle, for all legs and all flights. Original dataset.

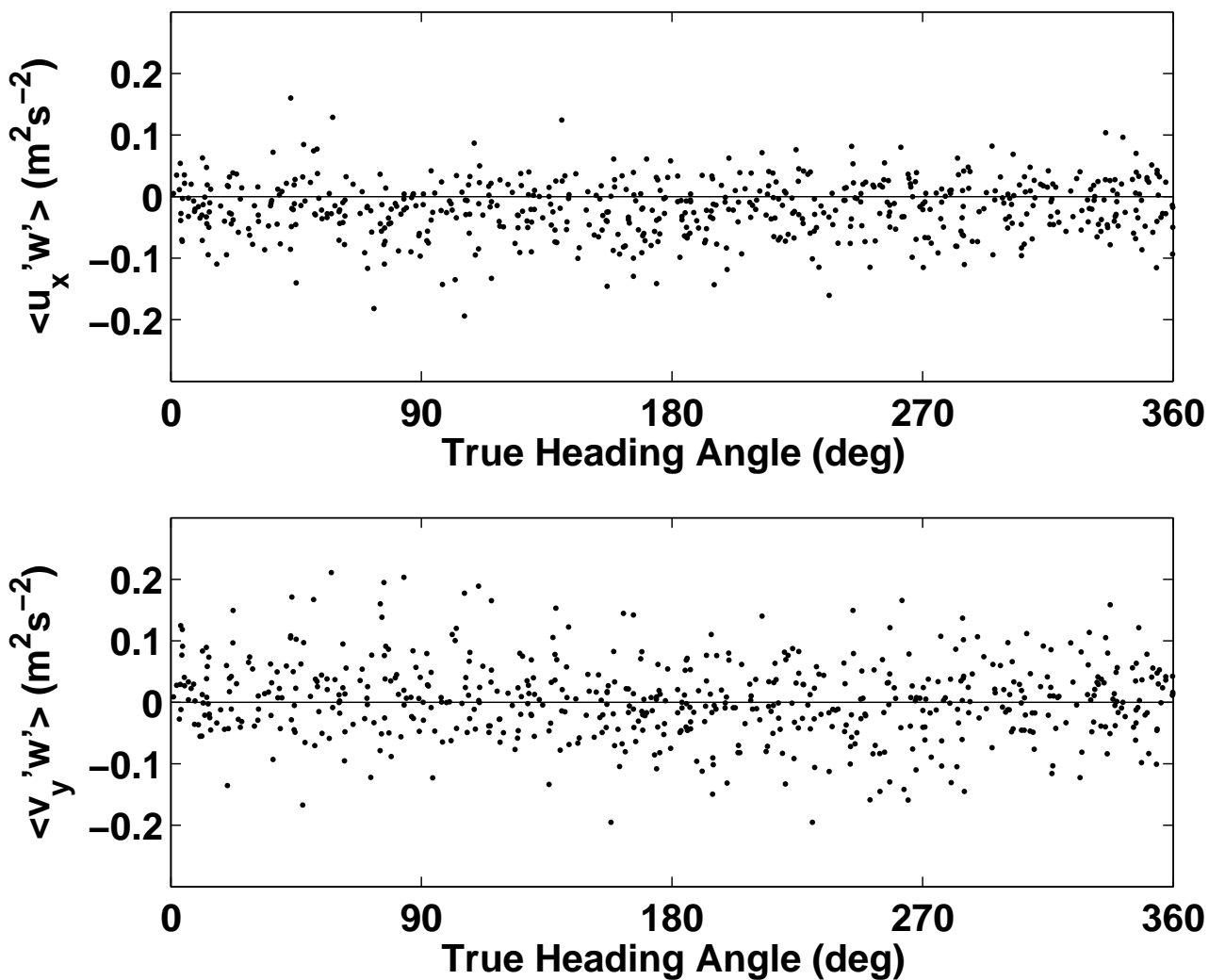


Figure 5: Longitudinal (top) and transverse (bottom) components of the vertical momentum flux, as a function of the true heading angle, for all legs and all flights. First new dataset (summer 2005).

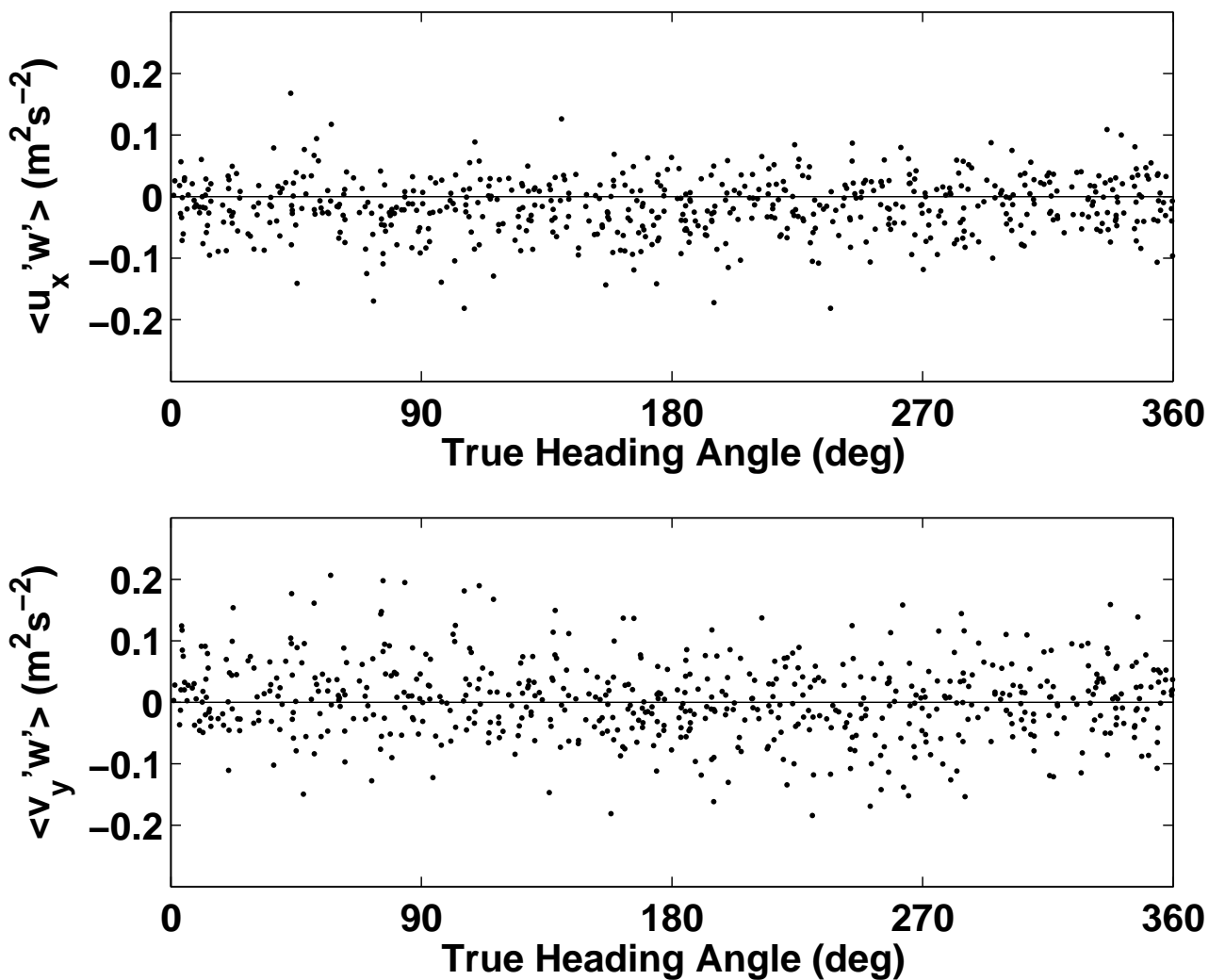


Figure 6: Longitudinal (top) and transverse (bottom) components of the vertical momentum flux, as a function of the true heading angle, for all legs and all flights. Second new dataset (fall 2007).

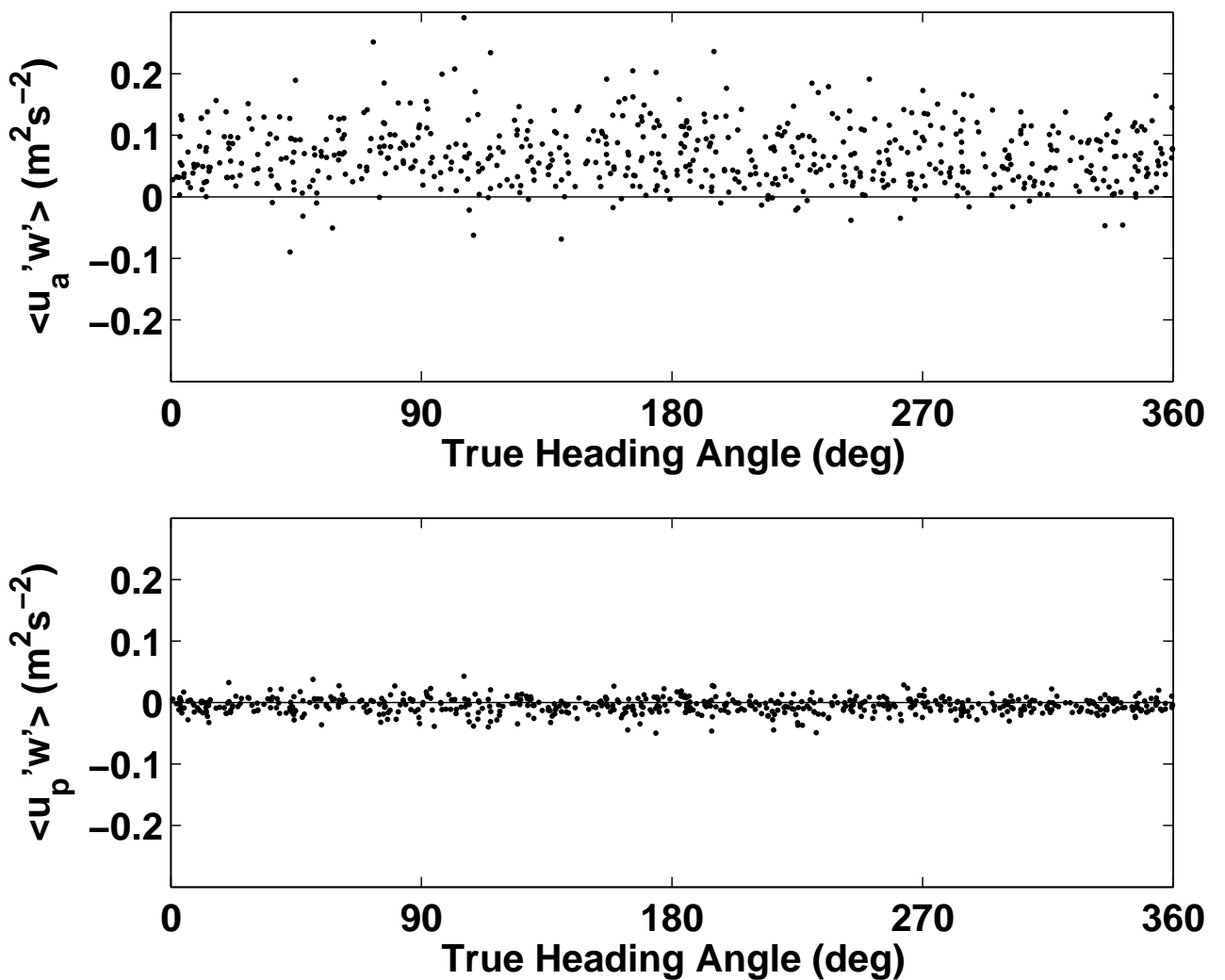


Figure 7: Covariance between the true air speed and the vertical velocity (top) and between the ground speed and the vertical velocity (bottom), as a function of the true heading angle, for all legs and all flights. Original dataset.

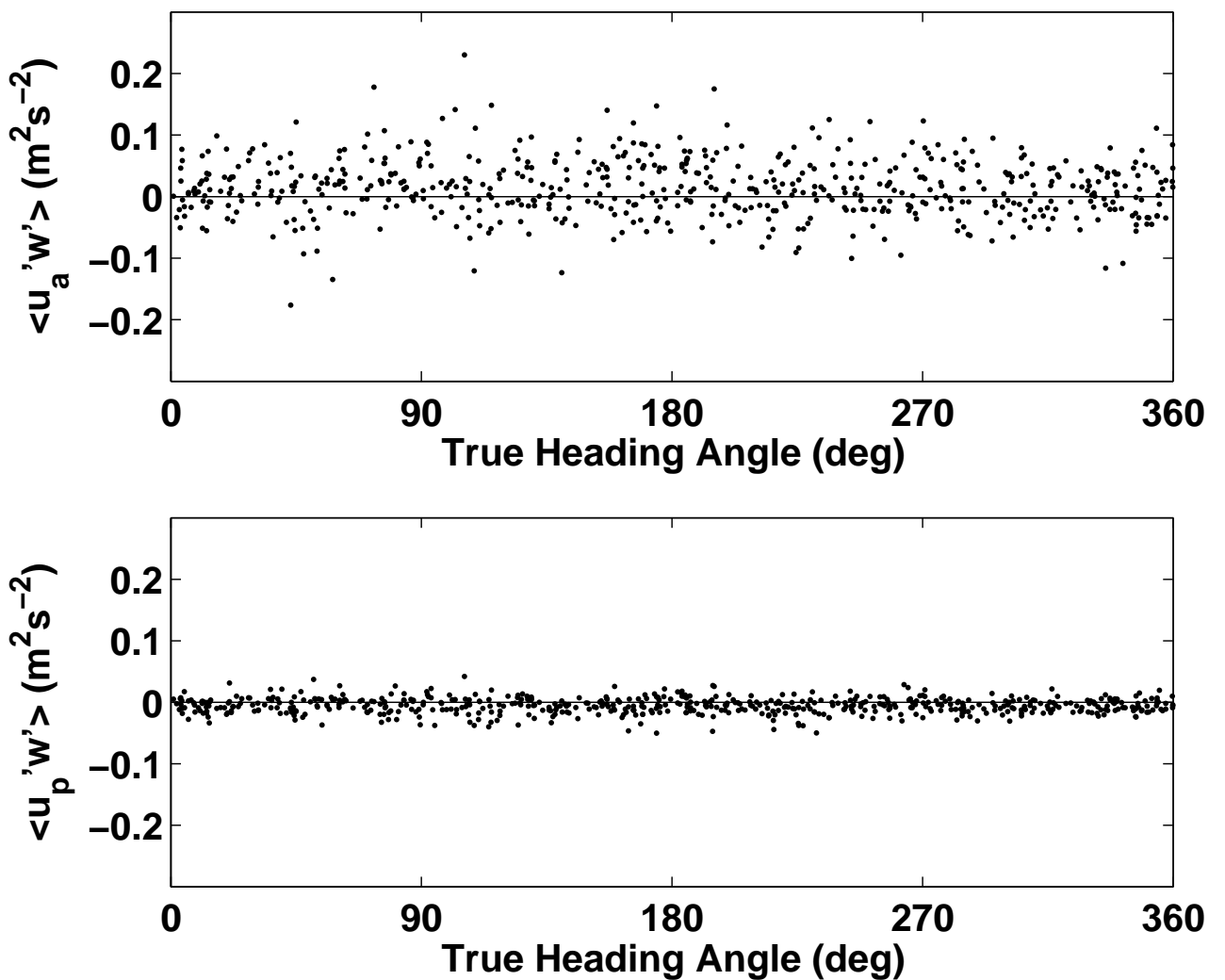


Figure 8: Covariance between the true air speed and the vertical velocity (top) and between the ground speed and the vertical velocity (bottom), as a function of the true heading angle, for all legs and all flights. First new dataset (summer 2005).

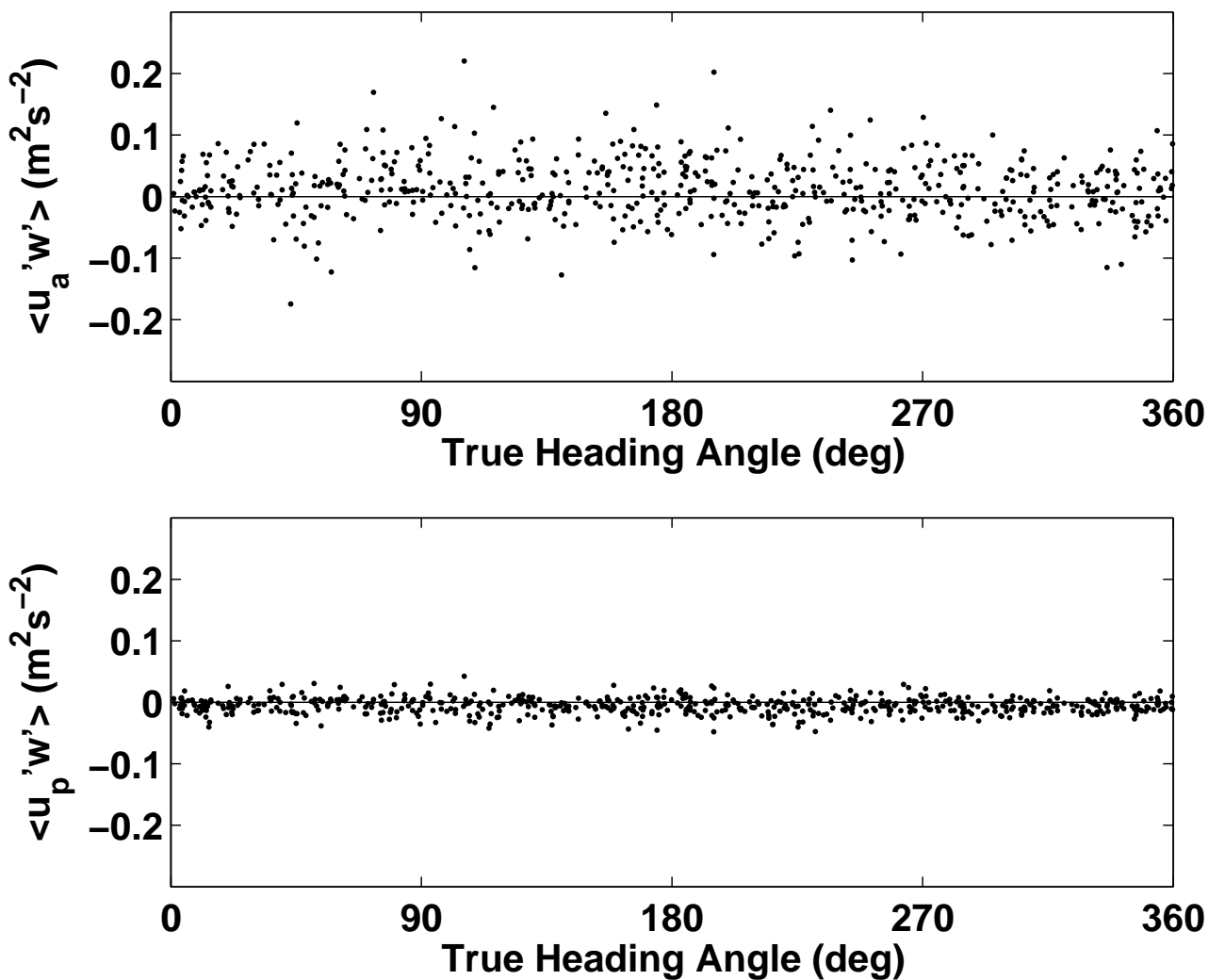


Figure 9: Covariance between the true air speed and the vertical velocity (top) and between the ground speed and the vertical velocity (bottom), as a function of the true heading angle, for all legs and all flights. Second new dataset (fall 2007).

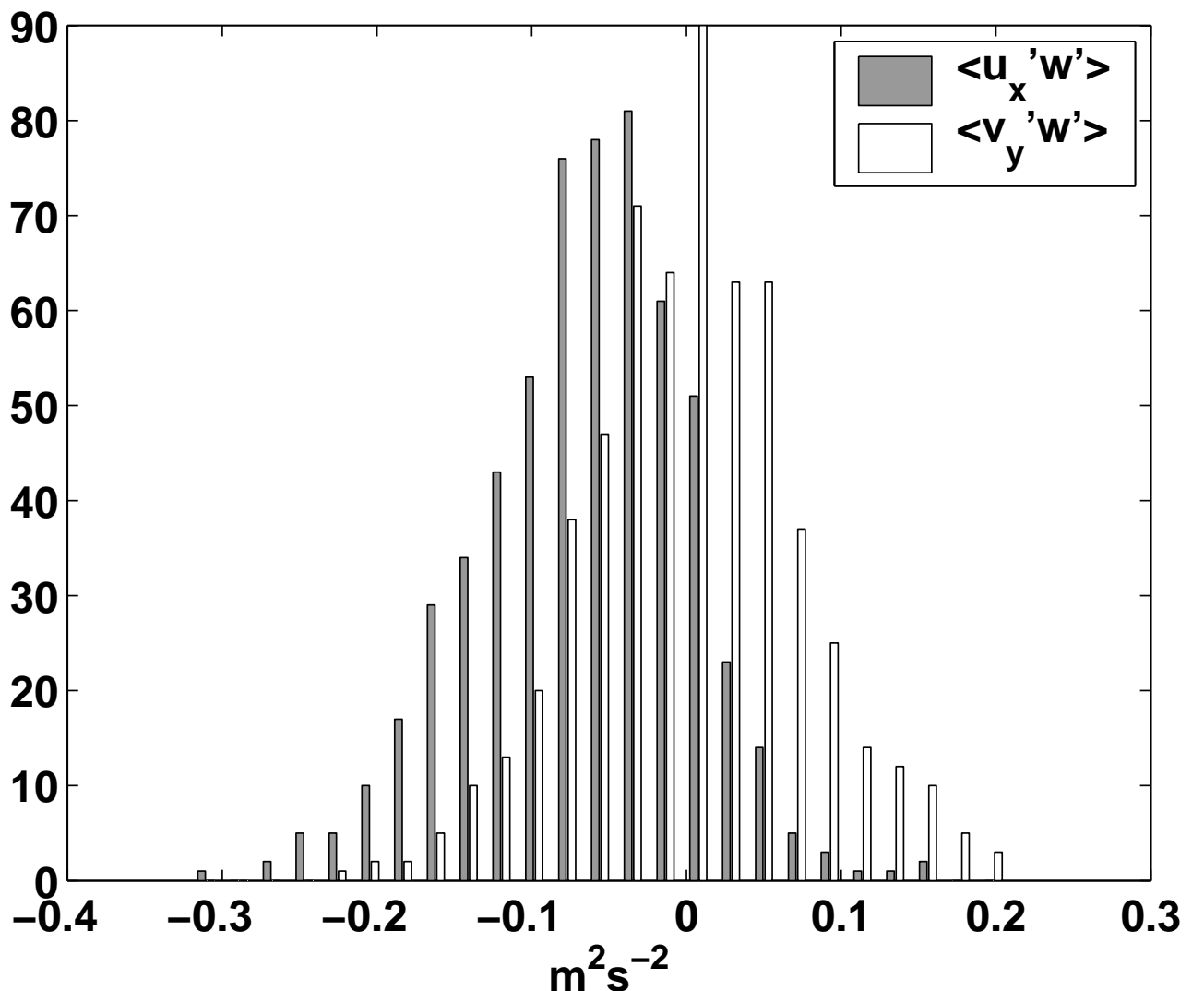


Figure 10: Distributions of the longitudinal (top) and transverse (bottom) components of the momentum flux. All legs and all flights are included. Old dataset.

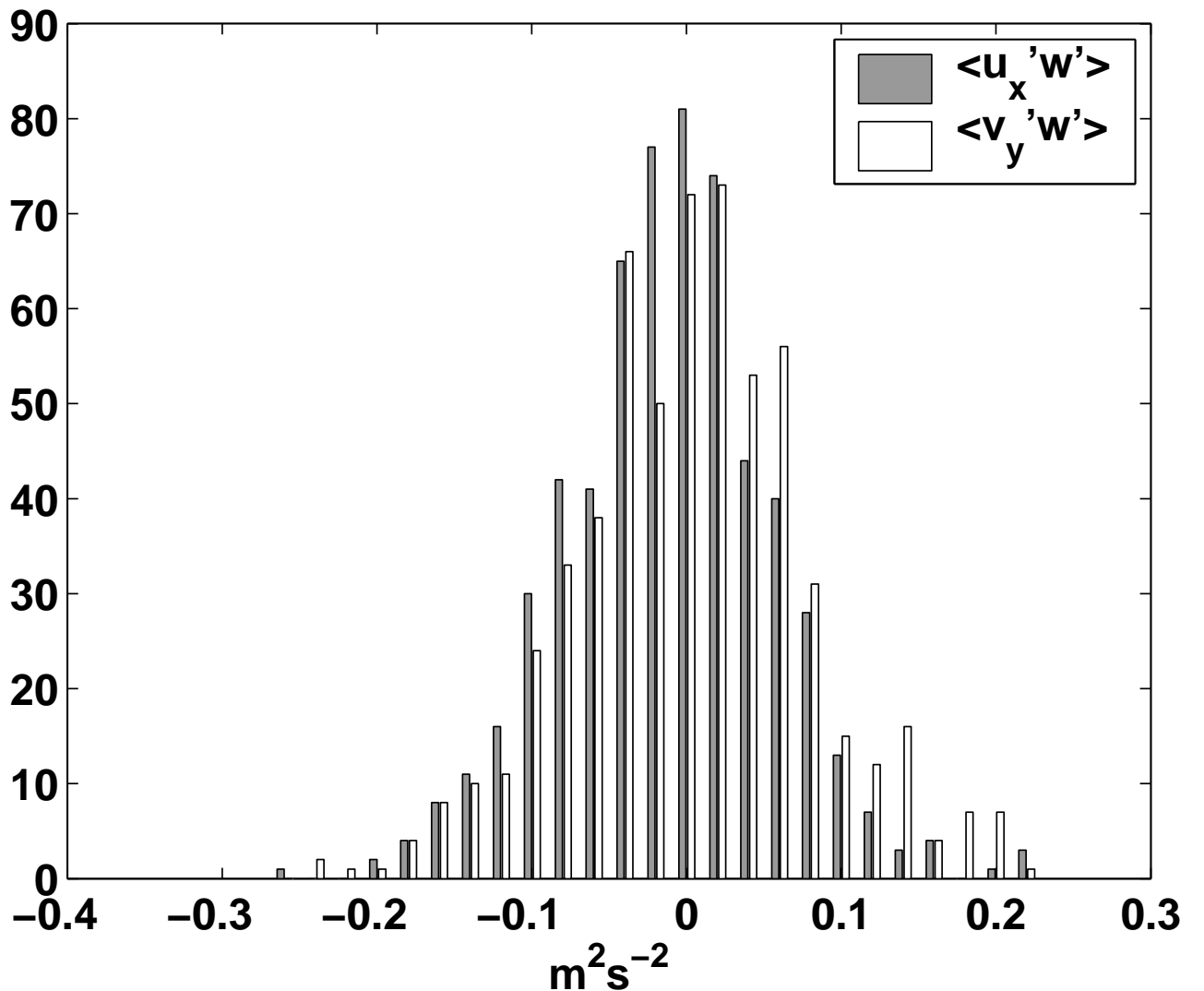


Figure 11: Distributions of the longitudinal (top) and transverse (bottom) components of the momentum flux. All legs and all flights are included. First new dataset (summer 2005).

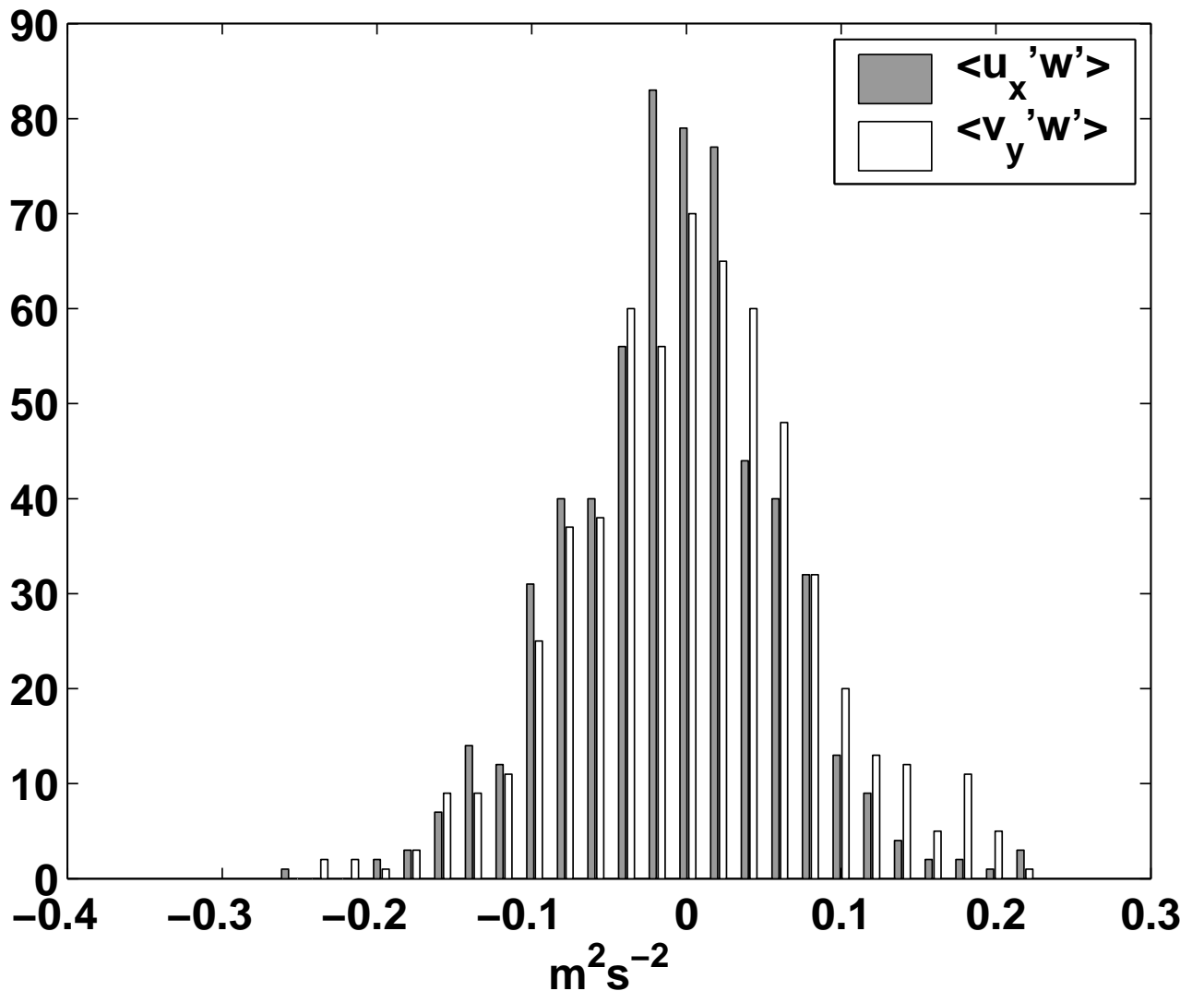


Figure 12: Distributions of the longitudinal (top) and transverse (bottom) components of the momentum flux. All legs and all flights are included. Second new dataset (fall 2007).

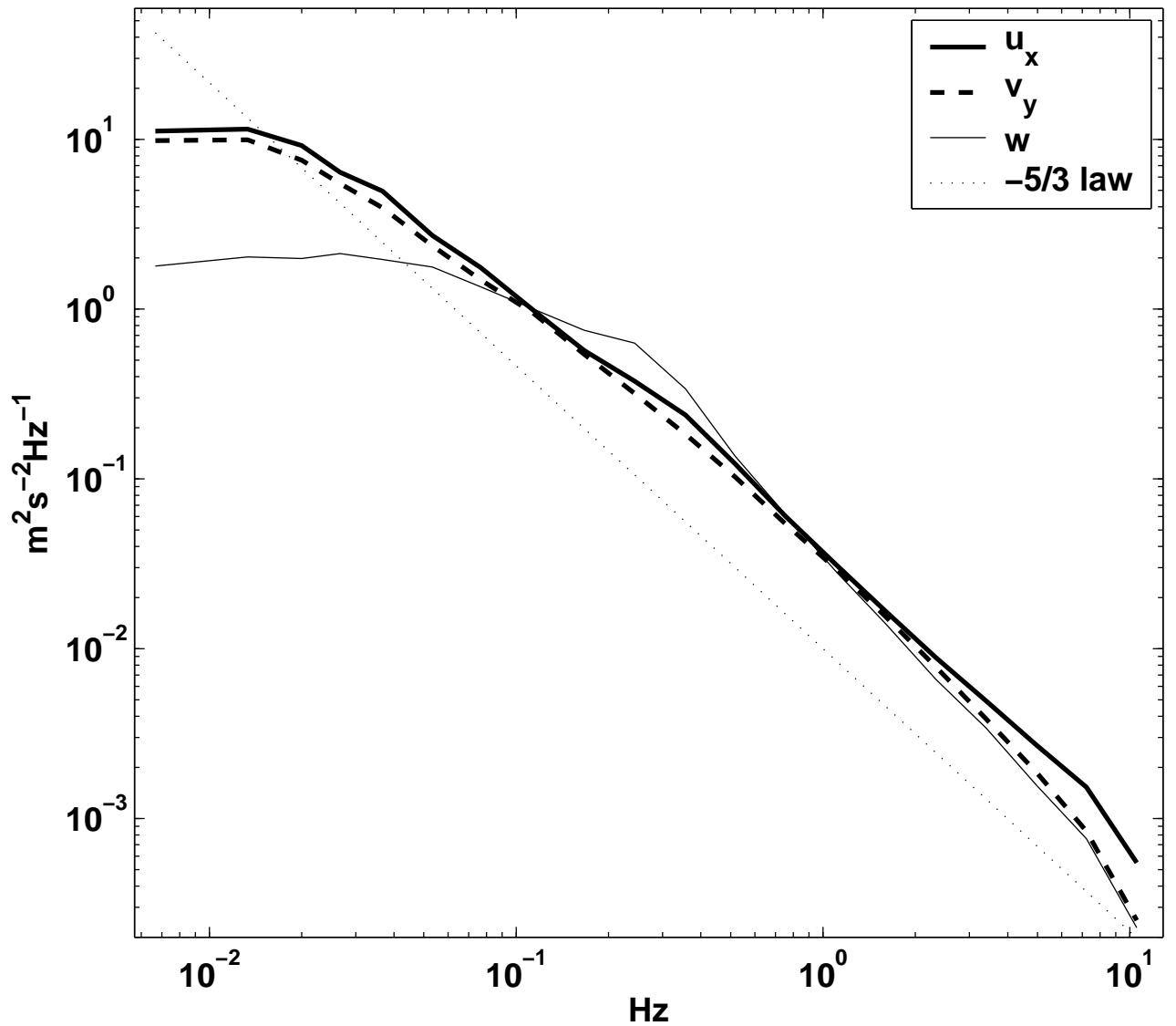


Figure 13: Mean spectrum of the three component of the wind (u_x , v_y , w) over all legs and flights, for the original dataset.

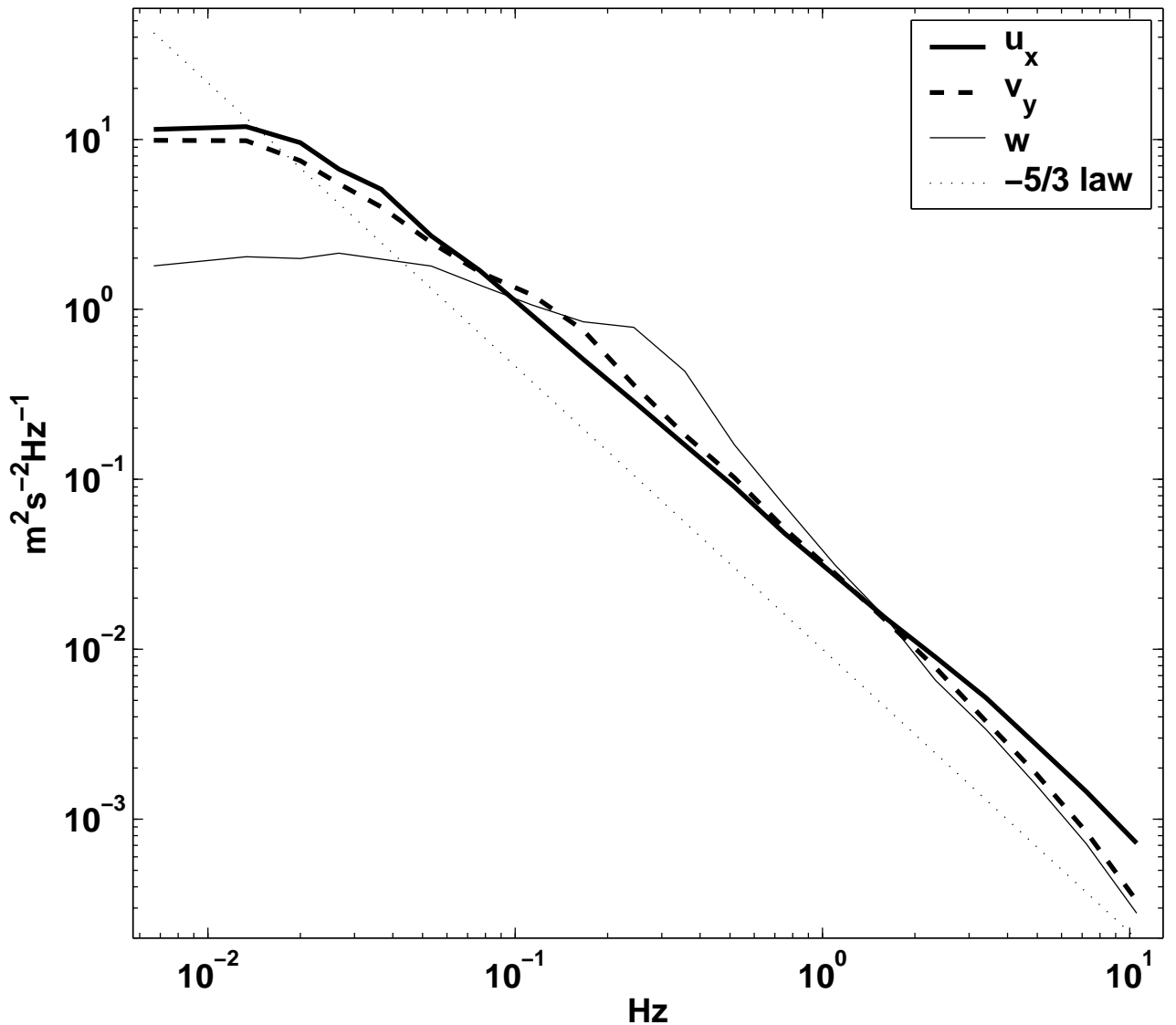


Figure 14: Mean spectrum of the three component of the wind (u_x , v_y , w) over all legs and flights, for the first new dataset.

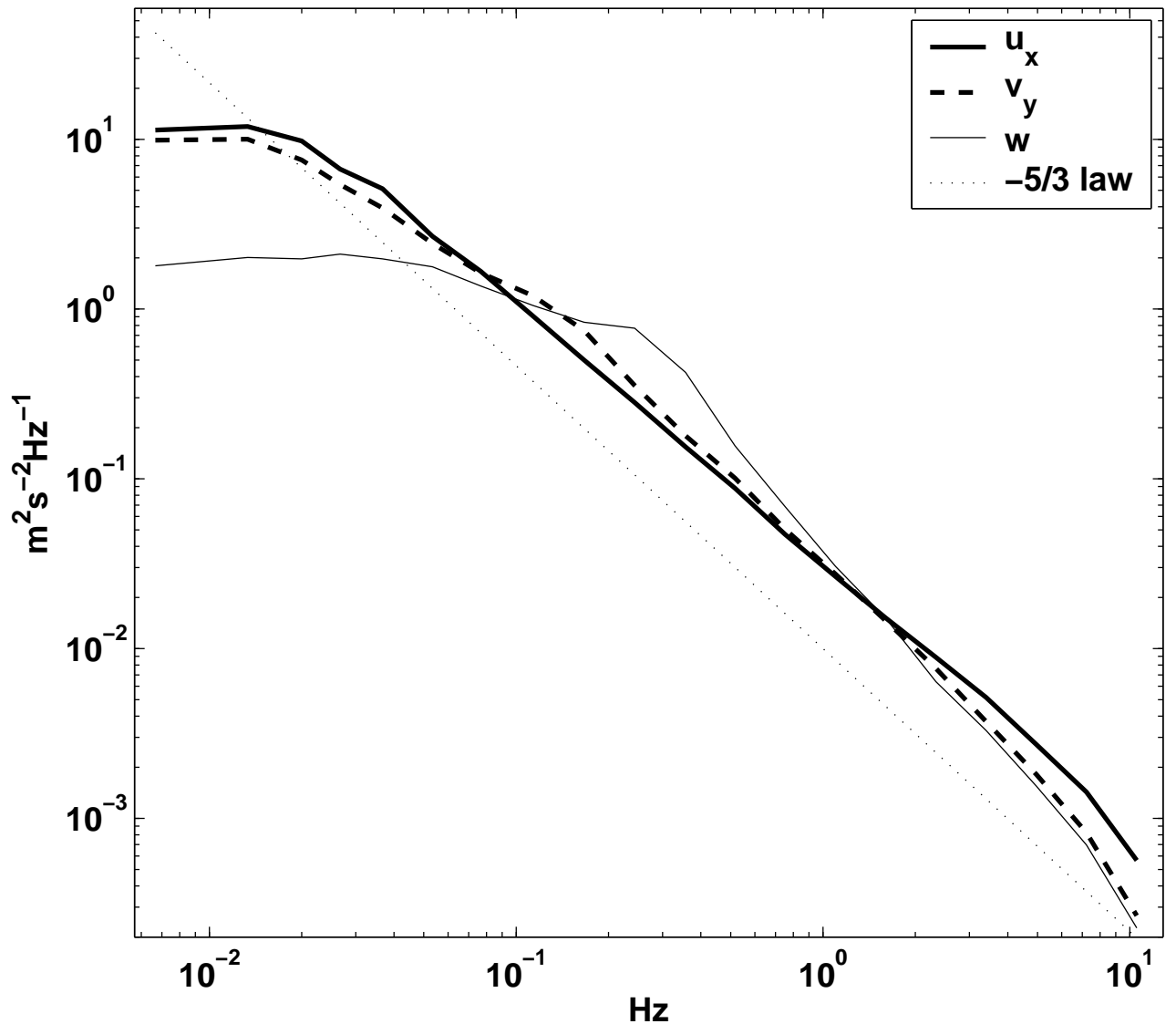


Figure 15: Mean spectrum of the three component of the wind (u_x , v_y , w) over all legs and flights, for the second new dataset.

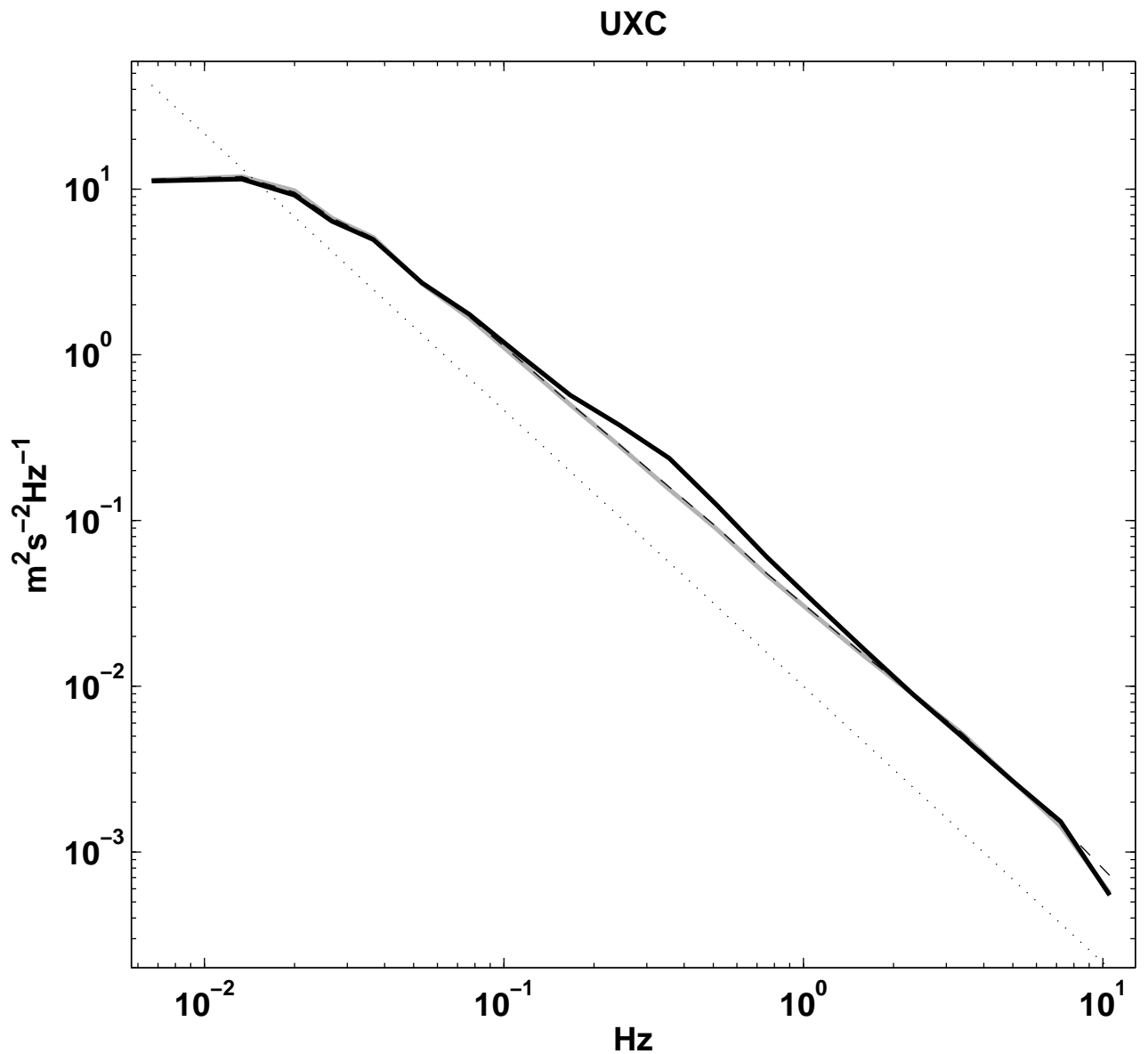


Figure 16: Mean spectrum of the longitudinal wind component over all legs and flights, for the three different datasets. Grey is the second new dataset, black is the original dataset, and dashed black line is the first new dataset.

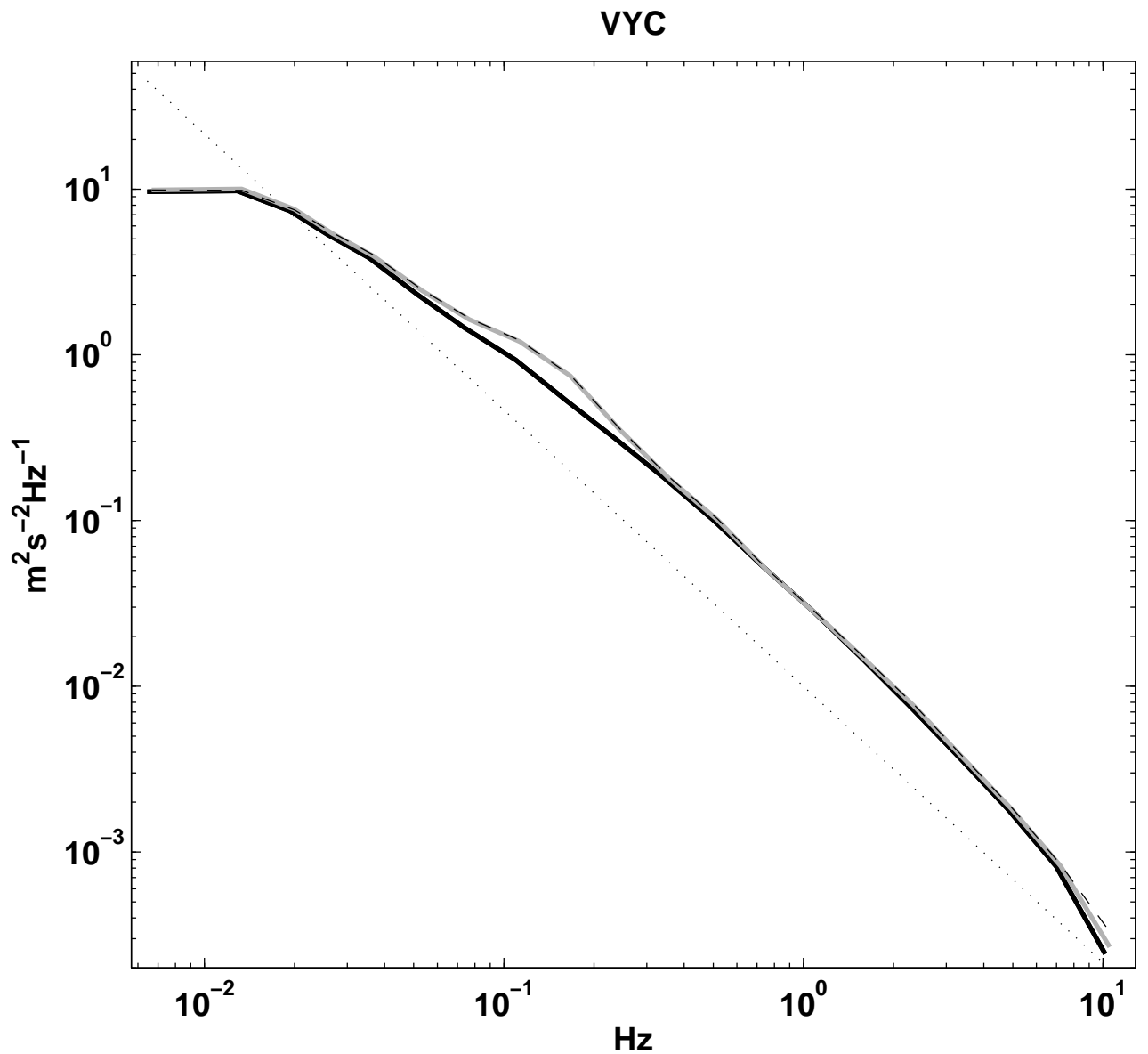


Figure 17: Mean spectrum of the transverse wind component over all legs and flights, for the three different datasets. Grey is the second new dataset, black is the original dataset, and dashed black line is the first new dataset.

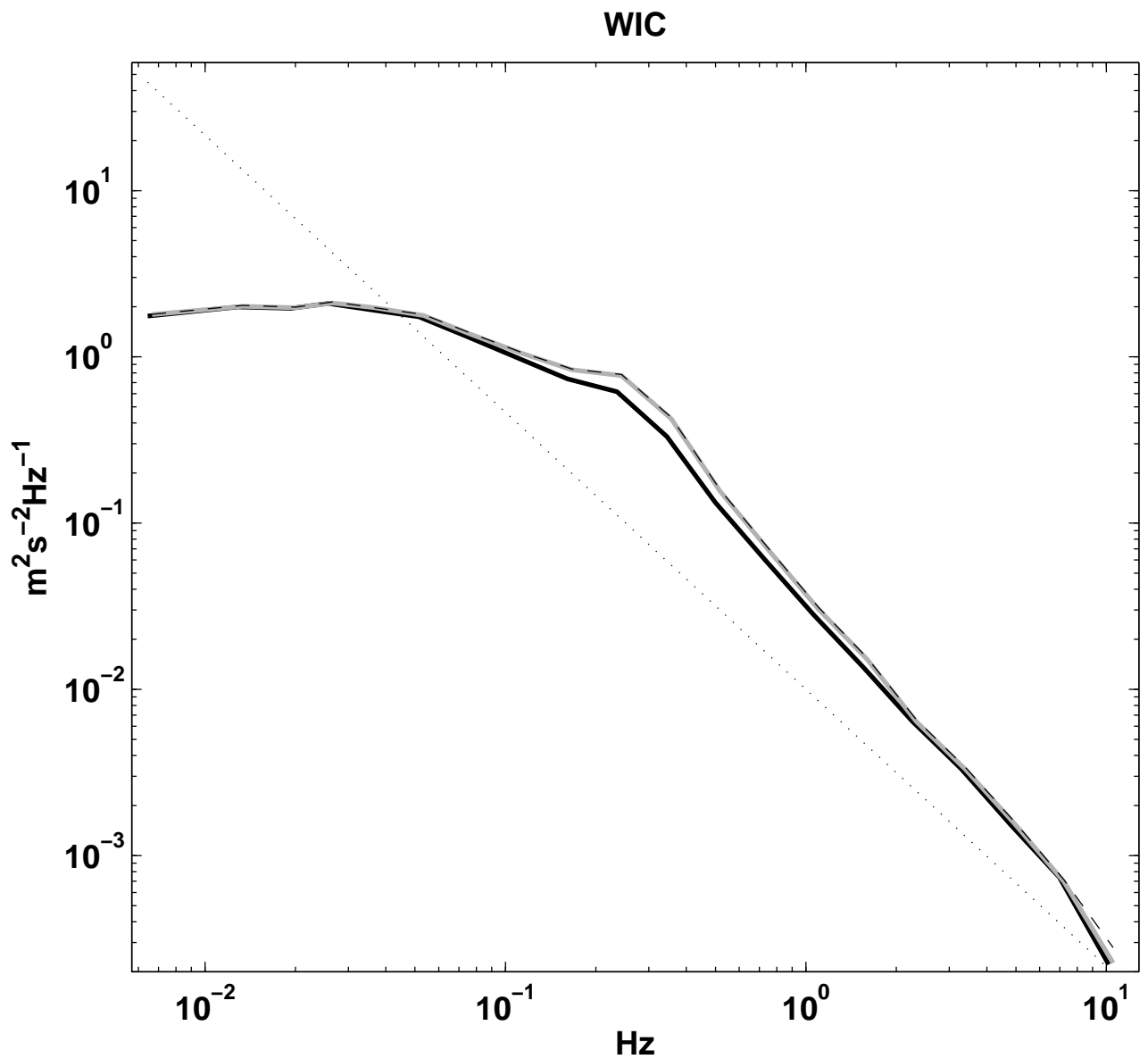


Figure 18: Mean spectrum of the vertical wind velocity over all legs and flights, for the three different datasets. Grey is the second new dataset, black is the original dataset, and dashed black line is the first new dataset.

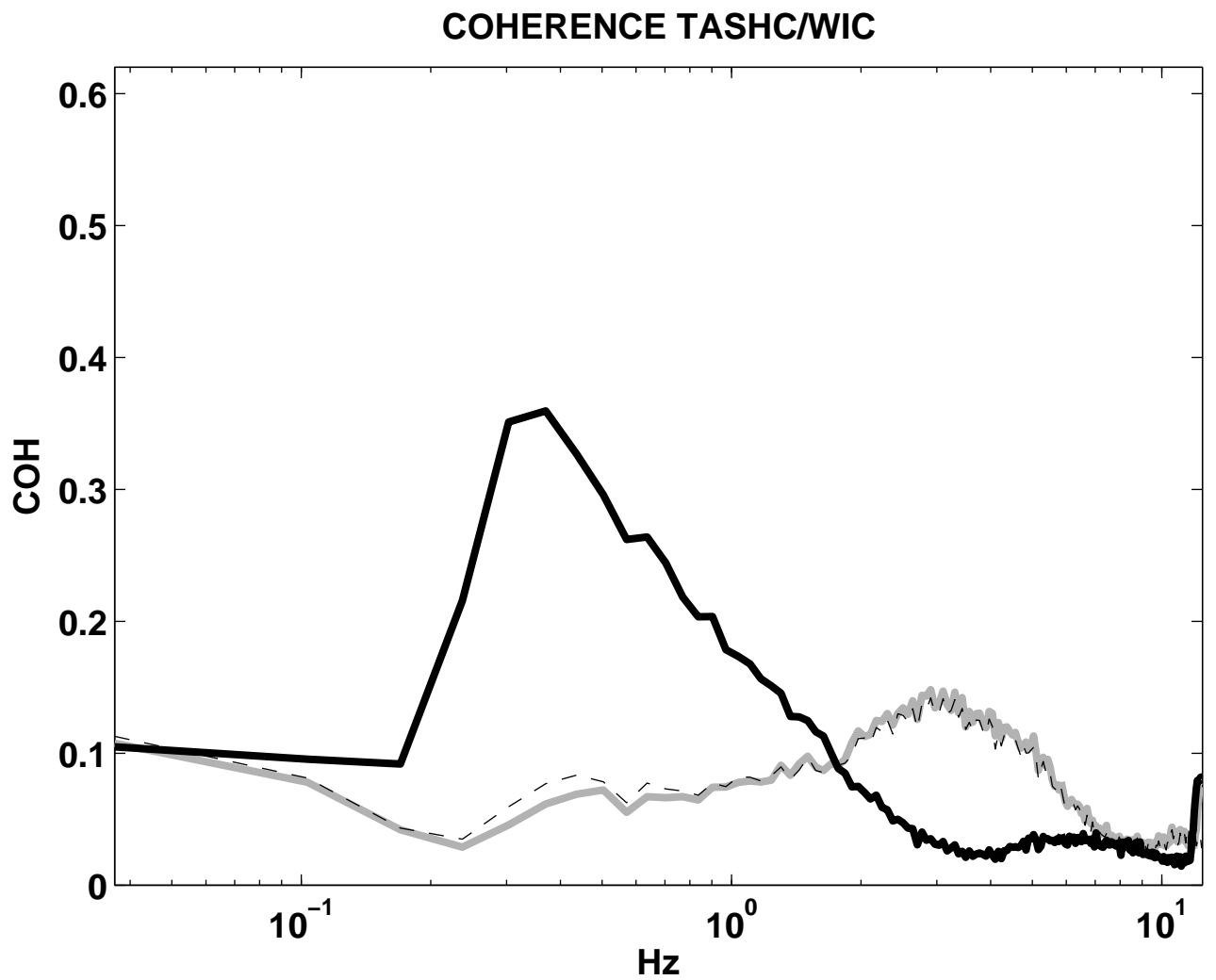


Figure 19: Mean coherence between the true air speed and the vertical velocity during all flights all legs, for the three different datasets. Grey is the second new dataset, black is the original dataset, and dashed black line is the first new dataset.